Large-Scale Convective Instability Revisited

KLAUS FRAEDRICH

Meteorologisches Institut, Universität Hamburg, Hamburg, Germany

JOHN L. MCBRIDE

Bureau of Meteorology Research Centre, Melbourne, Australia

(Manuscript received 22 June 1994, in final form 27 October 1994)

ABSTRACT

Linear convective instability is revisited to demonstrate the structurally different growth rates of disturbances in balanced and unbalanced models where diabatic heating is parameterized to be proportional to the vertical mass flux, and Ekman-type lower boundary conditions are introduced. The heating parameterization leads to an "effective static stability," which is negative when the vertical cumulus mass flux exceeds the total mass flux. This results in large-scale convective overturning. The appropriate horizontal scale is the usual Rossby deformation radius modified by the parameter $\sqrt{\gamma - 1}$, where γ is the ratio of cumulus to total mass flux. The unbalanced flow instability varies from zero growth ($\sigma = 0$) at finite horizontal scale (corresponding to twice the modified deformation radius $L = 2R$) to infinitely large values ($\sigma \to \infty$) at smallest scales ($L \to 0$). The growth of the related balanced model commences at the same scale ($L = 2R$) but attains infinitely large values on approaching the scale of the modified deformation radius $L = R$. This short-wave cutoff appears as a result of the changing vertical mass flux–heating profile associated with the Ekman boundary condition. Growth rates, horizontal length scales, and associated mass flux profiles are qualitatively supported by observations.

A feature of the solution is its dependence on vertical structure. Specifically, for each imposed vertical structure there are two solutions: one unbalanced corresponding to the cloud scale, and one balanced corresponding to the scale of the modified deformation radius. It is the thesis of this paper that the latter (large scale) solution represents a viable mechanism for the initial growth of either cloud clusters or tropical cyclones in nature.

1. Introduction

Lilly (1960), in an extension of the work of Haque (1952) and Syono (1953), constructed a linear perturbation model for the development of a tropical cyclone. The model is hydrostatic and nonviscous with a zero basic state; the distinguishing feature is the presence of a modified static stability whereby in the regions of upward vertical motion the static stability is that relevant to saturated ascent along a pseudoadiabat and so is negative. Despite being developed as an aid in understanding tropical cyclones, the unstable solutions were of internal gravity wave type (depending on the unbalanced response of the partial derivative of wind with respect to time to the pressure gradient force), and the growth rate asymptoted toward infinity with vanishing horizontal scale. It was thus interpreted by later authors (Kuo 1961, 1965; Charney and Eliassen 1964; Charney 1973; Yamasaki 1972; Asai and Nakasuji 1977; Ooyama 1982; Yoshizaki and Mori 1990) as being the instability governing the growth of cumulonimbus convection and thus a mathematical model for moist conditional instability. Charney and Eliassen (1964) and, independently, Ooyama (1964) proposed an alternate linear perturbation model for tropical cyclone development. The model geometry was essentially similar to that of Lilly (1960), with hydrostatic, nonviscous governing equations, zero basic state, and an initial region of upward motion surrounded by a laterally unbounded region of downward motion. The instability mechanism, however, was distinctly different from that of Lilly (1960). The instability was present in the balanced set of equations, which means it was not of internal gravity wave type. An essential component of the instability was a parameterization of heating that included a component proportional to an Ekman boundary condition for vertical motion. Thus, the heating contained a proportionality to the model low-level vorticity field and was essentially different from the Lilly instability, which depended on the presence of a modified static stability (Mak 1981). This second instability formulated by Charney, Eliassen, and Ooyama is referred to as CISK (conditional instability of the second kind).

Corresponding author address: Dr. John L. McBride, Bureau of Meteorology Research Centre, GPO Box 1289K, Melbourne 3001, Australia.

In this paper, we return to the modified static-stability instability model of Haque and Lilly. We demonstrate that an effective or modified static stability can appear in the thermodynamic equation through the use of a mass-flux-based parameterization scheme appropriate to large-scale flow. In the presence of the Ekman boundary condition the resultant instability has both a balanced and an unbalanced solution. The balanced solution gives growth rates on the timescale of a day, and on length scales of several hundred kilometers. Both the growth rate and horizontal scale are related to the vertical structure of the initial perturbation. By comparison with vertical structures and horizontal scales of incipient tropical cyclones in nature, we propose that the balanced version of the model may be a viable mechanism for either tropical cyclone or tropical cloud cluster development in nature.

2. Governing equations and analysis

The governing equations for convective instability used in this study are the following set for inviscid, hydrostatic, slab-symmetric flow on an f plane in pressure coordinates with diabatic heating proportional to the vertical mass flux. They were used in the early 1950s and 1960s by Haque (1952) and Lilly (1960) as linear perturbation models before convective instability of the second kind (Charney and Eliassen 1964; Ooyama 1964; Mak 1981) was discussed:

$$\frac{\partial u}{\partial t} = fv$$

$$\lambda \frac{\partial v}{\partial t} + fu = -\frac{\partial \phi}{\partial y}$$

$$\frac{\partial v}{\partial y} + \frac{\partial \omega}{\partial p} = 0$$

$$\frac{\partial}{\partial t}\left(-\frac{\partial \phi}{\partial p}\right) - \omega S = \frac{QR^*}{c_p p}. \qquad (1)$$

Here u, v, ω are the velocity components in the x, y, p directions; ϕ is geopotential height; and all four dependent variables are perturbations about a zero basic state. Further, S is the static stability; Q is the diabatic or cumulus heating; R^* is the gas constant; and λ is a trace indicator set to $\lambda = 1$ or $= 0$ according to whether or not the model describes unbalanced or balanced flow.

a. Parameterization of convection

There are many observational studies demonstrating that for large-scale motions in the Tropics the diabatic heating associated with mesoscale convective complexes approximately balances the adiabatic cooling associated with large-scale upward vertical motion (McBride 1981a; Frank 1980; Mapes and Houze 1992). However, when large-scale disturbances develop, the surface pressure goes down by 1–2 hPa (McBride 1981a). Through hydrostatic considerations, this means the heating has slightly exceeded the cooling. Thus, we introduce the concept of an *effective static stability,* defined mathematically as

$$\text{Effective Static Stability} \equiv (1 - \gamma)S, \qquad (2)$$

where the coefficient γ is defined as the ratio of diabatic heating to adiabatic cooling:

$$\gamma \equiv -\frac{QR^*}{c_p p} \Big/ \omega S. \qquad (3)$$

Thus, γ is positive if condensational heating occurs. Substituting (3) into the thermodynamic equation of set (1) gives a cumulus parameterization of the mathematical form

$$\frac{QR^*}{c_p p} = -\omega \gamma S. \qquad (4)$$

This formulation may be interpreted in terms of a mass flux convective parameterization scheme following the classical model of Fraedrich (1973), Arakawa and Schubert (1974), McBride (1981b), and others. The diabatic heat source due to a cloud mass flux M_C is virtually realized by the large-scale disturbance in its cloud-free environment through "compensating subsidence" of the cloud mass flux acting on the ambient static stability S:

$$\frac{QR^*}{c_p p} = M_C S \quad \text{or} \quad \gamma = \frac{M_C}{M} = \frac{M - M_E}{M}. \qquad (5)$$

That is, the mass fluxes, $M_C = -a\omega_C$ and $M_E = -(1 - a)\omega_E$, in the cloud and cloud-free areas, a and $(1 - a)$, are balanced by the total $M = -\omega$. First-order estimates may be based on climatological scaling: (i) radiative cooling of 1K day^{-1} is compensated by large-scale subsidence in the cloud-free environment where $M_E \sim (1 - a)$ 30 hPa day^{-1}; and (ii) the total mass flux in a tropical cyclone is about $M = -\omega \sim +200$ hPa day^{-1} (averaged over the scale of the disturbance, which a posteriori has an approximately 325-km radius). This determines the total mass balance (5) and yields a measure for the parameter $\gamma \sim M_C/M \sim 1.14$ representative for a convectively active area: $a \approx 0.1$.

Mathematically, the parameterization (4) is equivalent to that used by Haque (1952) and Lilly (1960). In their studies, the parameter $(1 - \gamma)S$ is a moist static stability corresponding to the difference between the atmospheric lapse rate and the moist-adiabatic lapse rate. Thus, their condition for instability was that γ exceed 1, corresponding to a conditionally unstable stratification. In the present model, the actual parametric condition required is that the diabatic heating slightly exceed the adiabatic cooling.

b. Solution procedure

Now an omega equation may be derived, which, after nondimensionalization of the horizontal and vertical coordinates $y = y^*R$ and $p = p^*P$ where $P = p_B - p_0$ (p_0, p_B being pressures at the top and bottom of the domain) and making use of the expression $e^{\sigma t}$, yields the following form:

$$-\omega_{y^*y^*} + \left(\lambda\frac{\sigma^2}{f^2} + 1\right)\omega_{p^*p^*} = 0, \tag{6}$$

where asterisked subscripts denote partial derivatives with respect to the nondimensional independent variables.

A modified Rossby radius of deformation, $R = \sqrt{S(\gamma - 1)}P/f$, has been introduced for convenience. Separation of the variables $\omega(p^*, y^*) = \omega(p^*)W(y^*)$ yields

$$\frac{W_{y^*y^*}}{W} = \left(\lambda\frac{\sigma^2}{f^2} + 1\right)\frac{\omega_{p^*p^*}}{\omega} = -m^2. \tag{7}$$

The separation constant m^2 represents the vertical scale in terms of a vertical wavenumber m.

The vertical boundary conditions lead to constraints that determine the instability of the flow and the growth rate of initially small amplitudes. There is vanishing mass flux $\omega(p = p_0) = 0$ at the top of the domain associated with two different types of lower boundary conditions at $p = p_B$.

(i) The vertical mass flux at the lower boundary vanishes:

$$\omega = 0. \tag{8}$$

(ii) An Ekman-type lower boundary condition can be derived from the assumption that the vertical mass flux through the top of the boundary layer is proportional to the geostrophic vorticity at the top of the boundary layer:

$$\omega = \frac{-K}{P}\frac{f}{\sigma}(\lambda\sigma^2/f^2 + 1)\omega_{p^*}, \tag{9}$$

where the constant of proportionality K is taken as the half-depth of the boundary layer (Charney 1973, chapter 13). It is worth commenting that this makes no assumption about balance (or geostrophy) in the interior of the fluid. It simply assumes that the adjustment time of the boundary layer is very rapid, so that an instantaneous balance between friction, pressure gradient, and Coriolis can be assumed in the boundary layer. This can be done even when no balance is assumed in the fluid interior because the adjustment time of the interior fluid is slower (Charney 1973).

The solution of (7) for horizontal structure satisfying both symmetry and maximum mass flux at $y = 0$ is

$$W(y^*) = \cos ky^*. \tag{10}$$

The solution for the vertical structure (satisfying the upper boundary condition) is

$$\omega(p^*) = \sin mp^*, \tag{11}$$

with $0 \leq p^* \leq 1$, so the value $m = \pi/2$ yields a vertical half-sine profile from a value of 0 at the top of the model to a maximum heating of 1 ($mp^* = \pi/2$) at the top of the boundary layer. Conversely, when $m = \pi$, the heating has a full vertical sine profile (i.e., from 0 to π) with maximum heating in the middle of the layer ($0 \leq p^* \leq 1$).

For consistency, the horizontal and vertical scales k and m are linked to the growth rate σ/f through substitution of (10), (11) into the omega equation (7):

$$k^2 = m^2\left(\lambda\frac{\sigma^2}{f^2} + 1\right). \tag{12}$$

Application of either lower boundary condition to the set (11), (12) eliminates one of the parameters (k, m), so that we can relate either scale directly to the growth rate σ.

Treating first the zero mass flux lower boundary condition (8), we obtain $m = \pi$ (or integer multiples of π), so that

$$\lambda\frac{\sigma^2}{f^2} = \frac{k^2}{\pi^2} - 1. \tag{13}$$

This is mathematically equivalent to the classical solution of Lilly (1960) and will be analyzed in section 4b.

The application of the Ekman lower boundary condition (9) at $p^* = 1$ and some algebra gives the relation

$$\lambda\frac{\sigma^2}{f^2} + A\frac{\sigma}{f} + 1 = 0, \tag{14}$$

where

$$A = \frac{P}{K}\frac{\tan m}{m} \quad \text{and} \quad m = k\Big/\left(\lambda\frac{\sigma^2}{f^2} + 1\right)^{1/2}. \tag{15}$$

This leads to a set of Ekman-influenced instabilities according to whether or not the flow in the interior of the system is considered balanced ($\lambda = 0$) or unbalanced ($\lambda = 1$). Thus, we have three unstable solutions: (i) Eq. (13), (ii) Eq. (14) with $\lambda = 0$, and (iii) Eq. (14) with $\lambda = 1$. In the following section, we present the relationships between horizontal scale, vertical scale, and growth rate for each instability.

3. Convective instabilities

a. Unbalanced without Ekman boundary condition

We consider first the case with zero mass flux at the lower boundary, which has the scale–growth relationship (13). This instability has been extensively analyzed [see, e.g., the Type I solutions of Lilly (1960);

Yoshizaki and Mori (1990)] and is commonly associated with cumulus and cumulonimbus convection.

Putting $\lambda = 1$, the instability diagram (Fig. 1, curve I) shows the normalized growth rate σ/f versus horizontal wavenumber k, inversely related to the normalized length scale or half-wavelength L/R representing the size of the (cloudy) area of upward motion and convective heating. The growth rate increases with horizontal wavenumber from zero growth at $k/\pi = 1$, where the upward mass flux area attains the scale of the modified deformation radius R, to infinity. For sufficiently large wavenumbers and growth rates a linear relation is attained, $\sigma/f \sim k/\pi$. As smaller scales are related to larger growth rates this convective instability has been associated with cumulus and cumulonimbus clouds. Note that this model provides a finite upper limit, $L = R$, of the horizontal scale, beyond which there is no growth. That is, convectively unstable unbalanced flow regimes without the Ekman boundary condition exist from zero size up to an area corresponding to the modified deformation radius.

The behavior of this model appeared to be unsatisfactory in explaining the development of larger-scale hurricane-like disturbances in the Tropics. Therefore, an Ekman-type boundary layer plus diabatic heating parameterized to be proportional to the mass flux at the top of the boundary layer were introduced to balanced and unbalanced models. Although leading to convective instability of the second kind (Charney and Eliassen 1964; Ooyama 1964; Mak 1981), these amendments did not (at least in a simple format) reveal the short-wave cutoff required for convectively driven disturbances in the tropical atmosphere to grow most intensely at large scales. These disturbances were still favoring waves of short wavelength.

b. Large-scale convective instability: Unbalanced flow with Ekman boundary condition

In a similar sense we extend the instability analysis and include an Ekman-type lower boundary condition (to balanced and unbalanced flow regimes) but retain the diabatic heating to be proportional to the vertical profile of the vertical mass flux. The relationship between growth rate and scale is given by Eqs. (14) and (15). Setting $\lambda = 1$ gives a quadratic for the growth rate of convectively driven unbalanced perturbations with Ekman-type lower boundary.

Unstable perturbations, $\sigma > 0$, require $A < 0$ or $\tan m < 0$, which holds for $\pi/2 < m < \pi$ (and integer multiples). Substituting into (11), the vertical mass flux profile is the proportion of the sine wave from $mp^* = 0$ at the top of the atmosphere to $mp^* = m$ at the top of the boundary layer. Thus, the unstable vertical mass flux profiles have shapes ranging from a full $(0, \pi)$ to a half $(0, \pi/2)$ vertical sine profile. The instability relation (14)–(15) shows large and small growth rates (Fig. 1, curve II), which can be related to balanced and

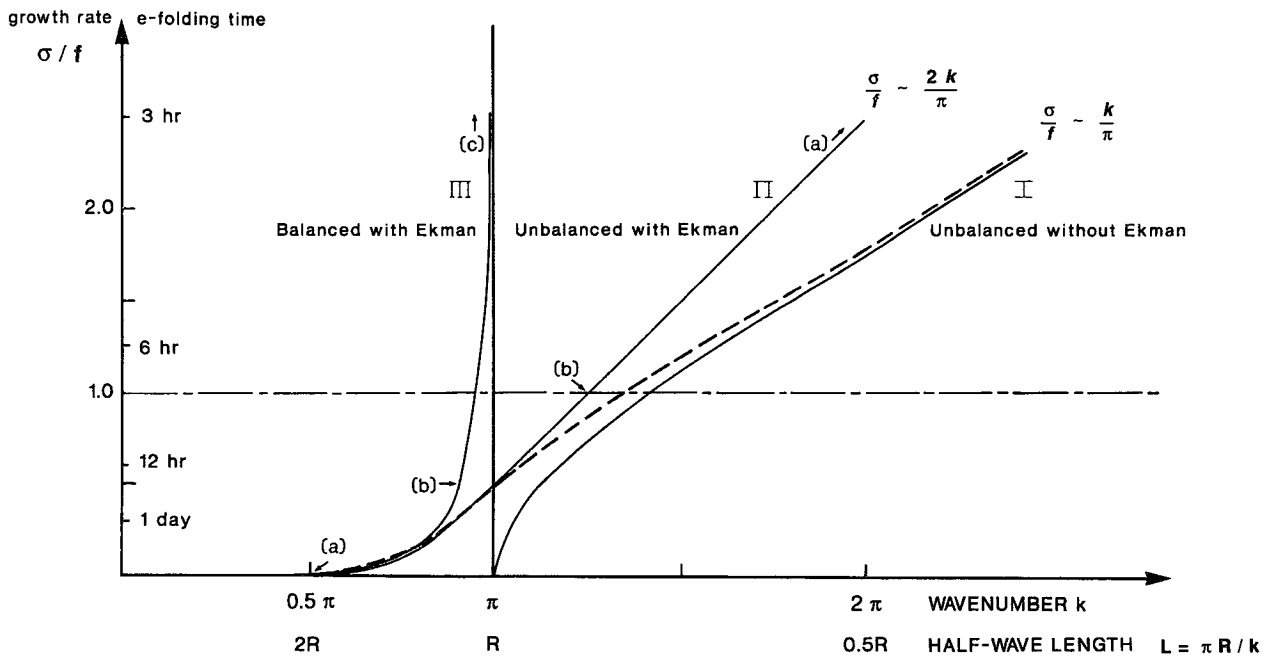

FIG. 1. The solutions for growth rate (normalized by f) versus the horizontal wavenumber k and the updraft length scale L (normalized by a modified Rossby deformation radius R). Curve I is unbalanced flow with a zero vertical motion lower boundary (i.e., the original conditional instability model). Curve II is for unbalanced flow with an Ekman lower boundary condition. Curve III is for the balanced model with an Ekman lower boundary. The dashed curve replaces curve II for the model with the alternative form of the Ekman boundary condition, as discussed in section 4b. The letters a, b, and c on curves II and III refer to the vertical structures shown in Fig. 2.

unbalanced flow regimes and the associated vertical mass flux/heating profiles (Fig. 2).

For large growth, $\sigma \gg f$, the system operates in the unbalanced flow regime, and spatial scales are small (k large). In the limit as $\sigma/f \sim -A \to \infty$, the vertical wavenumber $m \to \pi/2$ (using 15), corresponding to a half-sine $(0, \pi/2)$ vertical mass flux profile. In this part of the solution space the growth rate σ increases linearly with horizontal wavenumber $\sigma/f \sim 2k/\pi$, that is, at twice the rate found in the unbalanced flow regime without Ekman boundary layer.

For small growth, $\sigma/f \to 0$, $-A \to \infty$, the system operates in the balanced flow regime, also revealing a half-sine vertical mass flux profile with $m \to \pi/2$ in the limit of zero growth. This limit is associated with a finite horizontal wavenumber, $k = \pi/2$, corresponding to a half-wavelength $L = 2R$, which is twice as large as observed in the unbalanced flow regime without the Ekman boundary layer. That is, the Ekman boundary condition enhances the scale of the convectively unstable flow to twice the modified Rossby deformation radius. In the next subsection we show that this scale enhancement is related to the dynamics of balanced flow with lower Ekman boundary condition, which reveals maximum growth of unstable perturbations at the finite half-wavelength $L = R$ $(k = \pi)$ and thus a short-wave cutoff.

Through the quadratic (14), each vertical structure gives two growth rates, one in each of the fast and slow regimes, the slow occurring at large horizontal scales compared to the modified deformation radius, and the fast at small horizontal scales. In the slow regime, the growth rate curve almost overlays curve III (Fig. 1), corresponding to the solution from the balanced set of equations (next subsection). In the fast (unbalanced flow) regime, the growth rate curve is qualitatively similar to that of the classical Lilly–Haque solution (i.e., curve I). The separation between the regimes occurs at $A' = -2$: This point is associated with a growth rate equivalent to the inertial or Coriolis frequency $\sigma' = f$, a marginal vertical wavenumber $m' \sim 0.903\pi \sim 2.84$, and a horizontal half-wavenumber $k' = m'\sqrt{2}$ or $k'/\pi \sim 1.3$ corresponding to a length scale $L' \sim 0.8R$, which characterizes the size of the convectively active area.

c. *Large-scale balanced flow* ($\lambda = 0$)

For balanced flow the condition for growing initial perturbations can be derived from (14)–(15) with $\lambda = 0$:

$$\frac{\sigma}{f} = -\frac{K}{P} k \cot k \quad \text{with} \quad k = m. \tag{16}$$

The instability graph is presented in curve III of Fig. 1, increasing from zero at horizontal half-wavenumber $k/\pi = 0.5$ (or horizontal scale $L = 2R$) to infinitely large growth at $k/\pi = 1$ (or $L = R$). There is no growth at smaller scales (larger wavenumbers). The corresponding vertical mass flux and heating profiles can be inferred from the magnitude of the wavenumber $0.5 < k/\pi = m/\pi < 1$: zero growth corresponds to a half-

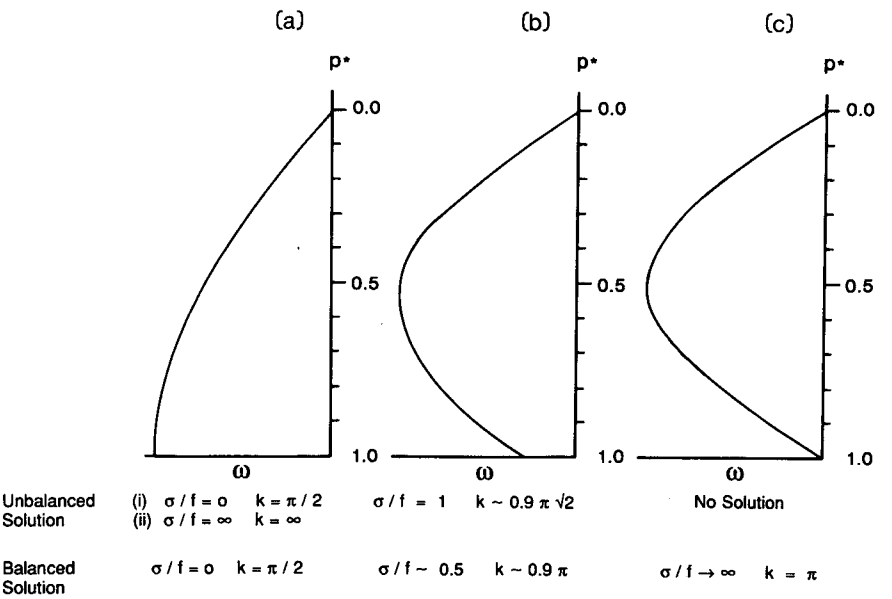

FIG. 2. Three vertical profiles of the vertical mass flux associated with different growth rates of unbalanced and balanced flow regimes with Ekman boundary conditions: (a) the most stable solution; (b) the limiting value for an unbalanced solution; and (c) the vertical profile corresponding to the most unstable solution of the balanced model.

sine $(0, \pi/2)$ profile, which tends to a full-sine profile $(0, \pi)$ in the limit of infinite growth at $k/\pi = 1$ or $L = R$.

Although a short-wave cutoff is achieved, it should be noted that balanced flow dynamics is applicable only for growth rates $\sigma^2/f^2 \ll 1$. As described in the previous subsection the unbalanced model has a limiting vertical wavenumber of $m' = 0.9\pi$ associated with horizontal wavenumber $k' = 0.9\pi\sqrt{2}$. In the balanced model this vertical structure leads to a solution of $\sigma/f = 0.5$ (associated with $k = 0.903\ \pi$) (see Fig. 2). This growth rate is an appropriate upper limit for the condition on σ^2/f^2; thus, the vertical wavenumber $m = 0.9\pi$ can be considered the limit for both versions of the model.

Two forcing mechanisms act in the large-scale convective instability: (i) Ekman spindown and (ii) condensational heating due to parameterized cumulus convection.

(i) Ekman spindown through vortex stretching is largest if there is mass outflow throughout the layer above the surface boundary and inflow in the boundary layer only. Ekman spindown vanishes if inflow and outflow balance above the boundary layer (showing no upward motion through the top of the boundary layer). These limits correspond to the half-sine $(0, \pi/2)$ and full-sine $(0, \pi)$ vertical mass flux profiles, respectively.

(ii) The condensational heating spinup creates the instability of the model. The associated growth rate is largest when Ekman spindown vanishes as a negative feedback process, that is, when inflow and outflow balance above the boundary layer [the $(0, \pi)$ sine profile]. The associated growth rate is zero when the Ekman spindown is at its maximum [the $(0, \pi/2)$ half-sine profile]. This argument explains, in qualitative terms, the extremes of the balanced flow instabilities and their association with the vertical structure.

The horizontal scale enters through the dynamics involved: the balanced flow regime without inertia gravitational modes adjusts to the Rossby radius of deformation at largest growth rate. In the unbalanced regime this is not the case: largest growth is associated with the half-sine $(0, \pi/2)$ profile related to Ekman spindown, but the growth due to heating is more effective in the limit of small horizontal scales associated with (inertia) gravity modes.

4. Alternative solutions

a. Conditional heating

The above solutions are derived from the use of the heating parameterization (4), where the coefficient γ has assumed a value constant throughout the domain. Thus, in the region of the convective disturbance the vertical mass flux is upward (i.e., ω is negative) so that the heating Q is positive. Conversely, in the surrounding region, ω is positive and Q is negative.

Many authors have solved the convective instability problem using "conditional heating" whereby the heating is set to zero beyond the disturbance half-width b:

$$\frac{QR^*}{c_p p} = -S\gamma\omega,$$

where

$$\gamma = +ve \quad |y| < b$$
$$\gamma = 0 \quad |y| > b. \tag{17}$$

Following this geometry, a separation of variables is still achieved, but the horizontal structure is trigonometric within the distance b and exponentially decaying outside. The solutions for growth rate as a function of horizontal scale are shown in Fig. 3. Curves I, II, and III are as in Fig. 1. The labels along the balanced curve III are the value of the intercept of the vertical structure function at the top of the boundary layer. Thus, if $\omega \sim \sin Dp$, these numbers are the value of Dp_B, where p_B is the pressure at the lower boundary. The solution procedure to obtain Fig. 3 involves matching solutions from the two domains ($|y| < b$, $|y| > b$) and therefore is more complicated than that described above. However, as can be seen in the figure, the solutions are qualitatively identical to those shown in Fig. 1, so that all of the interpretation and conclusions made above are unaffected by this extension to conditional heating.

b. An alternative form of the Ekman boundary condition

In section 2b the vertical motion at the lower boundary was assumed proportional to the geostrophic vorticity at the top of the Ekman layer, $\omega = -K\xi_G = -(K/f)\partial^2\phi/\partial y^2 = -(K/fP\sigma)(\lambda\sigma^2 + f^2)\partial\omega/\partial p^*$. A number of authors (e.g. Mak 1981; Fraedrich and McBride 1989) have made the alternative Ekman assumption that the vertical motion at the lower boundary is proportional to the actual vorticity ($\omega = -K\xi = K\partial u/\partial y$). For the reasons discussed in section 2b, we believe that the form of the lower boundary condition in Eq. (9) is more appropriate for the present study. It is instructive, however, to consider the solution obtained from the alternative version:

$$\omega = -K\xi = -\frac{Kf}{P\sigma}\omega_{p^*}. \tag{18}$$

Then Eq. (15) is unchanged, but (14) becomes

$$A\frac{\sigma}{f} + 1 = 0, \tag{19}$$

where, as before, $A = (P/K)(\tan m)/m$, with $m = k/\sqrt{\lambda\sigma^2/f^2 + 1}$. For this equation set, the balanced solution ($\lambda = 0$, curve III in Fig. 1) is unchanged.

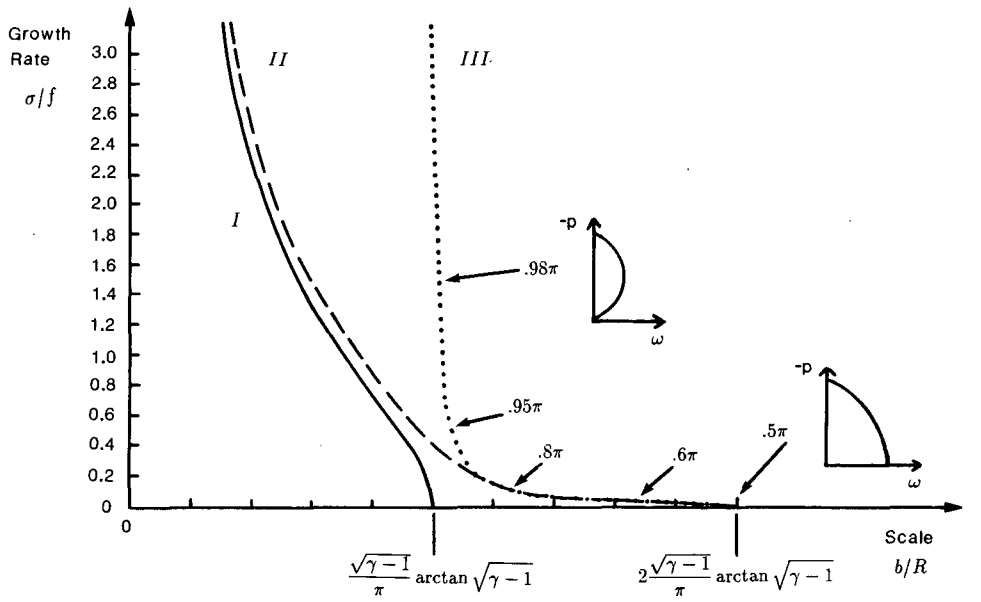

FIG. 3. Growth rate versus horizontal scale for the conditional heating form of the model. Curve I is for the unbalanced solution with zero lower boundary condition. Curve II is for the unbalanced solution with the Ekman boundary condition. Curve III is for the balanced solution with Ekman boundary condition. The numbers along curve III refer to the intercept of the vertical structure function at the lower boundary. The vertical structure for the heating (or for ω) is sketched at 0.98π and at 0.5π.

The instability relation for the unbalanced solution ($\lambda = 1$) is displayed as the dashed curve in Fig. 1. Unstable perturbations require $A < 0$ or $\tan m < 0$. Thus, the vertical structure function $m \in [\pi/2, \pi]$. However, the loss of the quadratic means that each vertical structure has a single solution. As m approaches $\pi/2$, the growth rate $\sigma \ll f$, and there is balanced dynamics. As seen in Fig. 1 the instability curve (dashed line) almost exactly overlays the solution for the balanced model (curve III).

At the other extreme $m \to \pi$ and $\sigma \to \infty$, and the solution rapidly approaches that of the classical unbalanced/no-Ekman model of Lilly and Haque (curve I).

5. Discussion and conclusions

In summary, the following points are noted on the properties of the large-scale convective instability explored in this note.

1) The traditional Lilly instability asymptotes at zero wavelength and is present only in the unbalanced set of equations.

2) The large-scale instability is present also in the balanced set and (when balanced) asymptotes at the deformation radius.

3) This change in properties is brought about by the presence of the lower Ekman boundary condition.

4) The horizontal structure and growth rate are determined by the vertical structure of the initial disturbance. It is this property that forces the solution to the large-scale balanced instability rather than the small-scale Lilly unbalanced instability.

5) Mak (1981) and Charney and Eliassen (1964) had the large-scale instability present in their models. Both authors had rejected it as unphysical. The basis for our present claim that it may operate in the atmosphere is our introduction of the concept of an "effective static stability" for large-scale flow. We derived the effective static stability through the use of classical cumulus mass flux concepts, but the key parametric assumption is that the diabatic (or convective) heating slightly exceeds the adiabatic cooling associated with large-scale ascent.

In the context of the last point, it is noteworthy that Gill (1982) also used the Lilly formulation to study tropical cyclones. Gill used the classical model (i.e., without an Ekman boundary condition) and externally imposed the horizontal scale so that he could study the three-dimensional structure of the solution.

The large-scale instability of the present paper is based on a representation of heating at a level in the vertical being proportional to vertical velocity at that same level, combined with an Ekman lower boundary condition. The solution for this model using the full (i.e., unbalanced) set of equations is represented by curve II of Fig. 1. Each point on the curve corresponds to a particular vertical structure of the heating, as represented by Fig. 2.

From some perspectives, this dependence on vertical structure could be considered a weakness of the model.

It means that the model does not select a free mode; one has to be preselected through specification of the vertical wavenumber m. This is not unreasonable as it is unlikely that in the tropical atmosphere the vertical heating structure would result from the properties of a large-scale dynamical instability mechanism. Rather, the vertical structure would be a function of the internal properties of the cumulonimbus ensemble, including the collective effects of individual cumulonimbus elements and stratiform anvils. To reduce this argument to its simplest example, the fact that the heating extends through the depth of the troposphere is due to the parcel buoyancy equation operating within the subgrid-scale (or parameterized) convective clouds.

Once the vertical structure is specified, however, the unbalanced solution (Fig. 1, curve II) has an interesting property. Each vertical structure yields two solutions: one in the balanced domain resembling the solution represented by curve III, and one in the unbalanced domain resembling the original Lilly model (curve I). This property is shown in Fig. 4, which shows the solution to the unbalanced model with Ekman boundary condition in $m-L$ space. As illustrated for the vertical structure $m = 0.7\pi$, there is one solution corresponding to the scale of individual cloud systems (i.e., an order of magnitude smaller than the modified deformation radius R) and one solution on the scale of cloud clusters and tropical cyclones (i.e., actually greater than R). Thus, this simple model actually duplicates the selection into two distinct horizontal scales, as occurs in the atmosphere. There is a bifurcation point in the solution (marked by the filled dot on Fig. 4) representing the limiting vertical wavenumber (m, approximately 0.903π).

It is our thesis that the balanced (or large scale, slow growth rate) part of the solution represents a viable instability for the initial growth of either a tropical cyclone or a tropical cloud cluster in nature. This statement may be justified through the following considerations.

(i) Mathematically, the instability stems from the combination of the Ekman lower boundary condition and the assumption that cumulonimbus heating at each level is proportional to the large-scale vertical motion at the same level. This latter assumption is verified in nature through the common observation that the apparent heat source Q_1 is approximately equal to $-\omega(\partial s/\partial p)$, where s is the dry static energy (Song and Frank 1983; McBride et al. 1989).

(ii) The growth rate and horizontal scale of the solutions to the balanced equations depend on the vertical structure of the ω profile in the initial disturbance. As shown in Fig. 2, the largest growth rates are associated with vertical profiles closest to a full-sine curve, while the slower growth rates are associated with a half-sine curve. Figure 5 shows observed vertical motion profiles from the tropopause (100 hPa) to the top of the boundary layer (850 hPa) for four stages of tropical cyclone development in nature. The incipient storm (stage D_1) approaches an almost full-sine structure with enhanced convergence above the boundary layer in agreement with the model, whereas in relative terms the boundary layer convergence increases with maturity of the storm, approaching an almost half-sine vertical mass flux profile for the fully developed storm (stage D_4).

(iii) At e-folding growth rates of the order of half a day, the horizontal half-wavelength or diameter of upward motion is approximately $1.1R$, where R is the modified Rossby radius of deformation. Using values of $f = 0.377.10^{-4}$ s^{-1}, $S = 10^{-2}$ m^2 s^{-2} hPa^{-2}, $P = 800$ hPa, $K = 100$ hPa, $\gamma = 1.12$, this corresponds to a diameter of approximately 750 km, which agrees well with observations. It should also be noted that while obeying the balance condition $\sigma^2/f^2 \ll 1$, this growth rate (1/half-day) is much faster than the Charney and Eliassen CISK growth rate, which is scaled by the Ekman timescale of approximately 6 days (Charney and Eliassen 1964; Fraedrich and McBride 1989).

These similarities with observations are a striking feature of the balanced flow model with cumulus heating proportional to the vertical mass flux. Therefore, we suggest that there may be a large-scale convective instability in balanced flow associated with an Ekman boundary condition and a convective heating proportional to the vertical mass flux, which to our knowledge, may have been left unnoticed.

As a final comment, it is appropriate to consider the relationship between this instability and other mechanisms for self-induced moist dynamics. As has been discussed throughout the paper, the large-scale convective overturning is a mechanism distinct from CISK. In recent years there has developed an extensive literature on two additional mechanisms: wave–CISK (e.g., Hendon 1988; Wang 1988; Rui and Wang 1990; Cho et al. 1994) and WISHE (wind-induced sea–air heat exchange) (Emanuel 1987; Neelin et al. 1987; Yano and Emanuel 1991). These two mechanisms also are distinct from that described here with regard to both physical or interpretive considerations and mathematical grounds. Mathematically, wave–CISK differs in that it depends on a vertical phase shift between heating and vertical motion (Bolton 1980; McBride and Fraedrich 1993). WISHE differs in that the heating is proportional to the actual wind speed at low levels, which means it will be dominated by the rotational wind at low levels in most large-scale flows. This is distinct from the heating at midlevels being proportional to the divergent wind at midlevels as is the case in the instability treated here. Both wave–CISK and WISHE share in common with the present instability the concept of an effective static stability as modified by the moist thermodynamics.

It is beyond the scope of the current paper to intercompare the three instabilities. Two of the most intrigu-

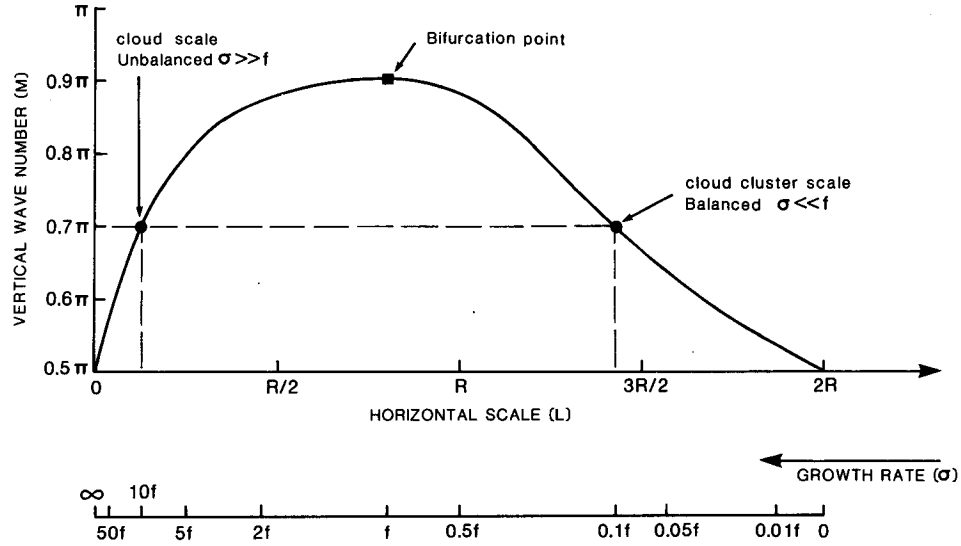

FIG. 4. The solution of unbalanced model with Ekman boundary condition (curve II of Fig. 1) in vertical wavenumber versus horizontal-scale space. Each vertical wavenumber m yields two solutions. They are measured along the lower axis in terms of horizontal scale (in units of the modified deformation radius R) or in terms of growth rate σ (measured in units of the Coriolis parameter f).

ing aspects of the present study are (i) the fact that each imposed vertical structure leads to a scale separation with one gravity-mode cloud-scale response and one large-scale balanced response; and (ii) the role played by Ekman frictional dynamics in forcing the solutions toward large horizontal scales. It would be worthy of investigation to determine whether similar roles are played by the vertical structure and by friction in the other two large-scale moist overturning mechanisms.

Acknowledgments. This project was begun during a visit by JMcB to the Freie Universität Berlin, for which we thank the Humboldt Foundation and the hospitality of the Freie Universität. It was completed during a number of short visits by KF to BMRC, for which we

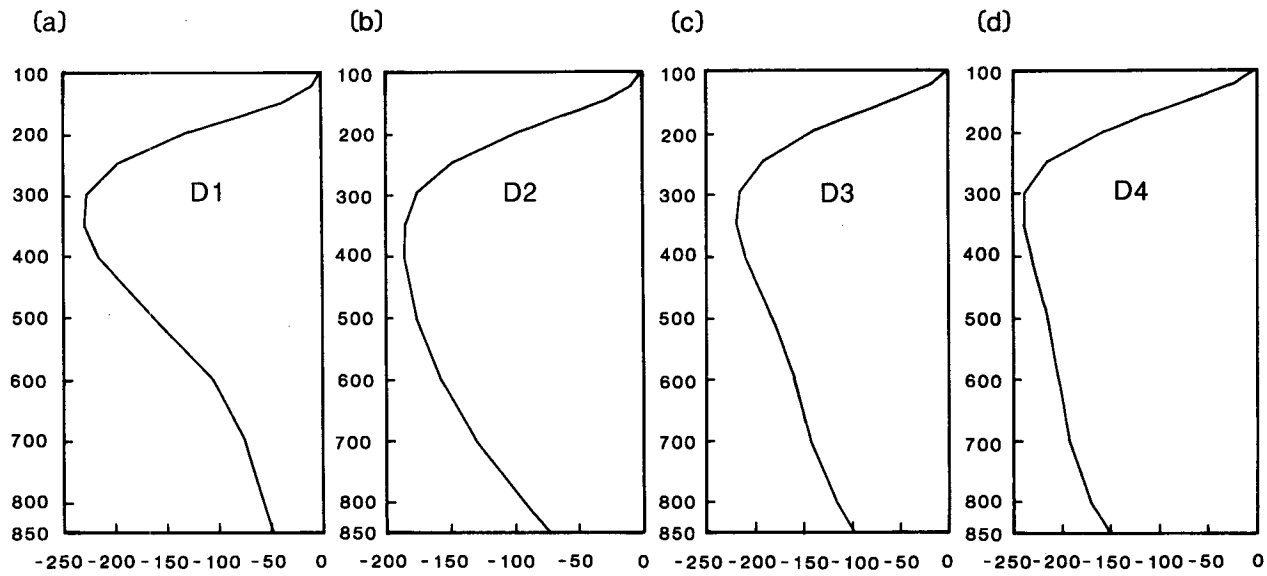

FIG. 5. Vertical mass flux profiles (hPa day^{-1}) for the northwest Pacific Ocean composite disturbances for four different stages of development (D1 to D4) from the incipient to mature typhoon. The values have been calculated from the 4-degree radius radial wind profiles in Fig. 5 of McBride (1981a).

thank the hospitality of that institution. It is also a pleasure to acknowledge Mankin Mak and W. M. Frank, both of whom contributed to this work through detailed discussions on an earlier version of the manuscript.

REFERENCES

Arakawa, A., and W. Schubert, 1974: Interactions of a cumulus cloud ensemble with the large-scale environment, Part I. *J. Atmos. Sci.,* **31,** 674–701.

Asai, T., and I. Nakasuji, 1977: On the preferred mode of cumulus convection in a conditionally unstable atmosphere. *J. Meteor. Soc. Japan,* **55,** 151–167.

Bolton, D., 1980: Application of Miles theorem to forced linear perturbations. *J. Atmos. Sci.,* **37,** 1639–1642.

Charney, J. G., 1973: Planetary fluid dynamics. *Dynamical Meteorology,* P. Morel, Ed., Reidel, 331–344.

——, and A. Eliassen, 1964: On the growth of the hurricane depression. *J. Atmos. Sci.,* **41,** 901–924.

Cho, H.-R., K. Fraedrich, and J. T. Wang, 1994: Cloud clusters, Kelvin wave–CISK, and the Madden–Julian oscillations in the equatorial troposphere. *J. Atmos. Sci.,* **51,** 68–76.

Emanuel, K. A., 1987: An air–sea interaction model of intraseasonal oscillations in the tropics. *J. Atmos. Sci.,* **44,** 2324–2340.

Fraedrich, K., 1973: On the parameterization of cumulus convection by lateral mixing and compensating subsidence, Part I. *J. Atmos. Sci.,* **30,** 408–413.

——, and J. L. McBride, 1989: The physical mechanism of CISK and the free-ride balance. *J. Atmos. Sci.,* **46,** 2642–2648.

Frank, W. M., 1980: Modulations of the net tropospheric temperature during GATE. *J. Atmos. Sci.,* **37,** 1056–1064.

Gill, A. E., 1982: Spontaneously growing hurricane-like disturbances in a simple baroclinic model with latent heat release. *Tropics in Atmospheric and Oceanographic Sciences: Intense Atmospheric Vortices,* L. Bengtsson and J. Lighthill, Eds., Springer-Verlag, 111–129.

Haque, S. M. A., 1952: The initiation of cyclonic circulation in a vertically unstable stagnant air mass. *Quart. J. Roy. Meteor. Soc.,* **78,** 394–406.

Hendon, H. H., 1988: A simple model of the 40–50 day oscillation. *J. Atmos. Sci.,* **45,** 569–584.

Kuo, H. L., 1961: Convection in a conditionally unstable atmosphere. *Tellus,* **13,** 441–459.

——, 1965: Further studies of the properties of cellular convection in a conditionally unstable atmosphere. *Tellus,* **17,** 413–433.

Lilly, D. K., 1960: On the theory of disturbances in a conditionally unstable atmosphere. *Mon. Wea. Rev.,* **88,** 1–17.

Mak, M., 1981: An inquiry on the nature of CISK, Part I. *Tellus,* **33,** 531–537.

Mapes, B., and R. A. Houze Jr., 1992: An integrated view of the 1987 Australian monsoon and its mesoscale convective systems. I: Horizontal structure. *Quart. J. Roy. Meteor. Soc.,* **118,** 927–963.

McBride, J. L., 1981a: Observational analysis of tropical cyclone formation. Part III: Budget analysis. *J. Atmos. Sci.,* **38,** 1152–1166.

——, 1981b: An analysis of diagnostic cloud mass flux models. *J. Atmos. Sci.,* **38,** 1977–1990.

——, and K. Fraedrich, 1993: The relevance of CISK to tropical cyclone development. Preprints, *Ninth Conf. on Atmospheric and Oceanic Waves and Stability,* San Antonio, Texas, Amer. Meteor. Soc., 207–210.

——, B. W. Gunn, G. J. Holland, T. D. Keenan, N. E. Davidson, and W. M. Frank, 1989: Time series of total heating and moistening over the Gulf of Carpentaria radiosonde array during AMEX. *Mon. Wea. Rev.,* **117,** 2701–2713.

Neelin, J. D., I. M. Held, and K. H. Crook, 1987: Evaporation–wind feedback and low-frequency variability in the tropical atmosphere. *J. Atmos. Sci.,* **44,** 2341–2348.

Ooyama, K. V., 1964: A dynamical model for the study of tropical cyclone development. *Geofis. Int.,* **4,** 187–198.

——, 1982: Conceptual evolution of the theory and modelling of the tropical cyclone. *J. Meteor. Soc. Japan,* **60,** 369–380.

Rui, H., and B. Wang, 1990: Development characteristics and dynamic structure of tropical intraseasonal convection anomalies. *J. Atmos. Sci.,* **47,** 357–379.

Song, J. L., and W. M. Frank, 1983: Relationships between deep convection and large-scale processes during GATE. *Mon. Wea. Rev.,* **111,** 2145–2160.

Syono, S., 1953: On the formation of tropical cyclones. *Tellus,* **2,** 179–195.

Wang, B., 1988: Dynamics of tropical low-frequency waves: An analysis of the moist Kelvin wave. *J. Atmos. Sci.,* **45,** 2051–2065.

Yamasaki, M., 1972: Small amplitude convection in a conditionally unstable stratification. *J. Meteor. Soc. Japan,* **50,** 465–482.

Yano, J.-I., and K. Emanuel, 1991: An improved model of the equatorial troposphere and its coupling with the stratosphere. *J. Atmos. Sci.,* **48,** 377–389.

Yoshizaki, M., and A. Mori, 1990: Another approach on linear theory of conditionally unstable convection: A forcing problem. *J. Meteor. Soc. Japan,* **68,** 327–333.